analytical chemistry

Article

Cite This: Anal. Chem. XXXX, XXX, XXX−XXX

pubs.acs.org/ac

Dual-Gated Transistor Platform for On-Site Detection of Lead Ions at Trace Levels

Shishir Venkatesh,[†] Tan Li,[†] Xiang-Sheng Wang,[‡] Chi-Chung Yeung,[§] Ke Pei,[∥] Qi-Jun Sun,[†] Wei Wu,[†] Robert K. Y. Li,[†] Michael H. W. Lam,[§] Paddy K. L. Chan,[∥] Jonathan J. Wylie,[⊥] and Vellaisamy A. L. Roy*[,†]

[†]State Key Laboratory for Millimeter Waves and Department of Material Science & Engineering, City University of Hong Kong, 83 Tat Chee Avenue, Kowloon, Hong Kong, S.A.R.

[‡]Department of Mathematics, University of Louisiana at Lafayette, Lafayette, Louisiana 70503, United States

[§]Department of Chemistry, City University of Hong Kong, 83 Tat Chee Avenue, Kowloon, Hong Kong, S.A.R.

[∥]Department of Mechanical Engineering, The University of Hong Kong, Pokfulam, Hong Kong, S.A.R.

[⊥]Department of Mathematics, City University of Hong Kong, 83 Tat Chee Avenue, Kowloon, Hong Kong, S.A.R.

Supporting Information

ABSTRACT: On-site monitoring of heavy metals in drinking water has become crucial because of several high profile instances of contamination. Presently, reliable techniques for trace level heavy metal detection are mostly laboratory based, while the detection limits of contemporary field-based methods are barely meeting the exposure limits set by regulatory bodies such as the World Health Organization (WHO). Here, we show an on-site deployable, Pb^{2+} sensor on a dual-gated transistor platform whose lower detection limit is 2 orders of magnitude better than the traditional sensor and 1 order of magnitude lower than the exposure limit set by WHO. The enhanced sensitivity of our design is verified by numerically solving PNP (Planck−Nernst−Poisson) model. We demonstrate that the enhanced sensitivity is due to the suppression of ionic flux. The simplicity and the robustness of the design make it applicable for on-site screening, thereby facilitating rapid response to contamination events.

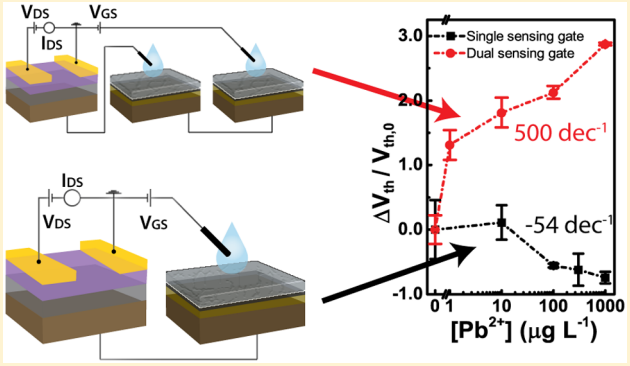

Heavy metals pose a serious threat to living organisms because of their toxicity and bioaccumulation.[1,2] Among the heavy metals, lead is the most widespread because of its historical use in paints, gasoline, and solder joints in water pipes. Although the usage of lead has been significantly reduced in recent years, lead in drinking water still continues to be a problem for numerous communities around the world.[3] Therefore, it is of paramount importance to monitor to levels of lead in drinking water so that any possible contamination can be rapidly identified and mitigated. The World Health Organization (WHO) recommends a guideline limit of 10 μg L^{-1} of total lead in drinking water.[4] Conventional testing methods for detection of trace concentrations include atomic adsorption spectroscopy (AAS), spectrophotometry, and inductively coupled plasma-mass spectroscopy (ICP-MS) among others.[4−9] However, these techniques require expensive laboratory-based equipment and trained personnel to operate them. Among field-based techniques, the most promising candidates are anodic stripping voltammetry and ion-selective electrodes.[10]

ISEs (ion-selective electrodes) are particularly interesting as they do not involve the use of the toxic dropping mercury electrode or the pretreatment of sample with bismuth which is required in anodic stripping voltammetry (ASV).[11−13] Historically, ISEs were plagued by poor mechanical durability and relatively high lower detection limits (LDL) limiting their use in on-site detection techniques. The mechanical durability of the ISE was upgraded with the development of the solid-contact ion selective electrode (SCISE), in which the conventional internal filling solution is substituted with a conducting polymer.

In addition, improvement in LDL of ISE was achieved by using low activity internal solutions,[14] establishment of preconditioning protocols[15,16] and transmembrane ionic flux control.[17−24] Because of the solid-contact, controlling the activity of internal filling solutions is not applicable for SCISEs. On the other hand, the LDL of SCISEs can be lowered by carefully controlling preconditioning procedures. Normally, ion selective membranes are activated through conditioning process in which the membrane is saturated with the analyte upon exposure to a

Received: February 21, 2018
Accepted: May 14, 2018

DOI: 10.1021/acs.analchem.8b00841
Anal. Chem. XXXX, XXX, XXX−XXX

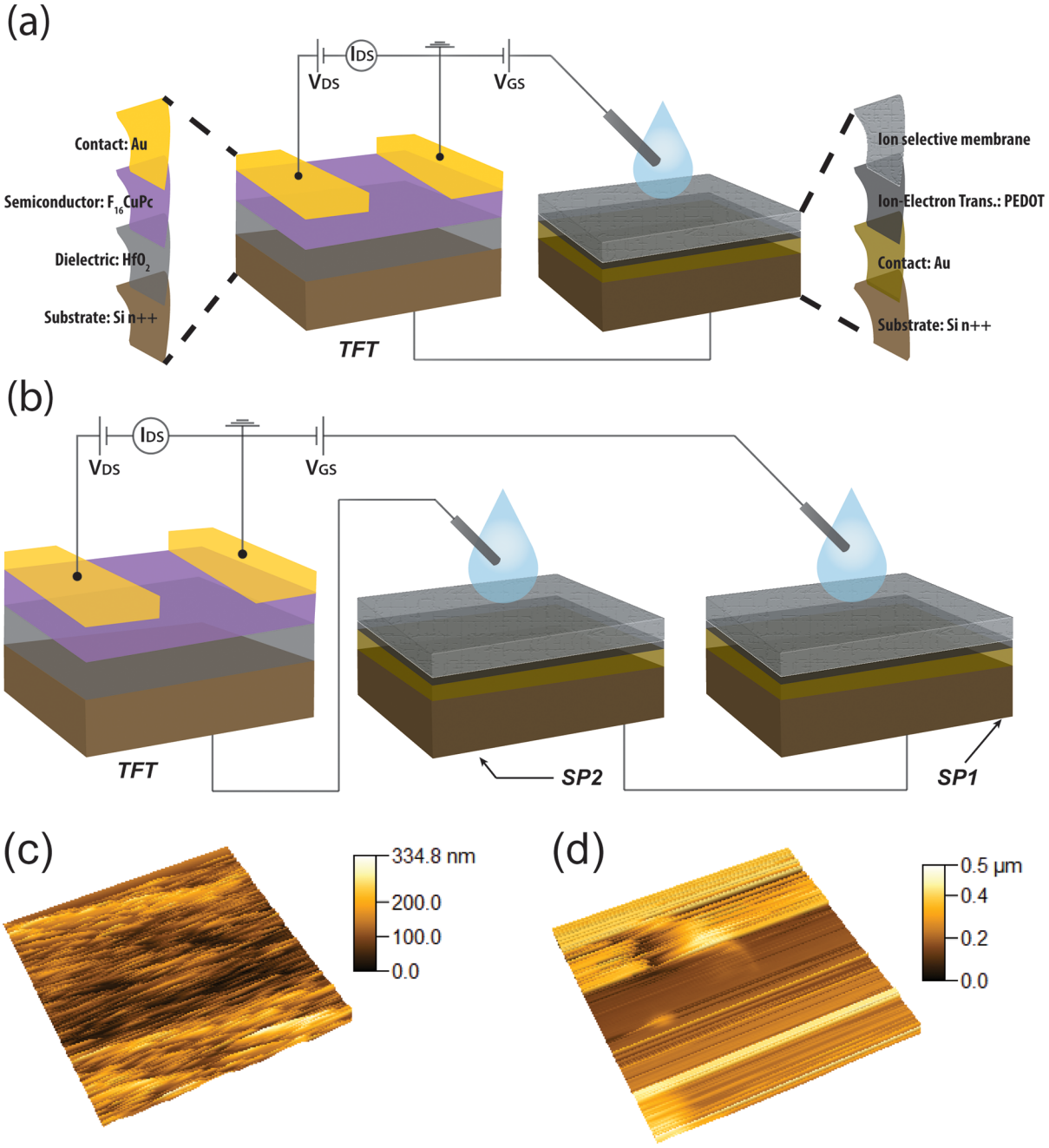

Figure 1. (a) Conventional single sensing gate field effect transistor. (b) Dual-sensing gate field effect transistor. 3D height profiles of the surface of the (c) PEDOT layer and (d) Pb^{2+} ion-selective membrane.

solution with high analyte concentration resulting in uptake of excess of analyte ions and also coextraction of counterions. This results in relatively high LDLs.[17] This limitation is overcome by using a second conditioning step in a low analyte concentration solution which removes the excess analyte and the coextracted ions in the membrane. Even using the two-step conditioning procedure presents some shortcomings at lower analyte concentrations. When the sample analyte concentration is higher than that in the solid-contact layer, analyte ions flux toward the solid-contact layer because of the concentration gradient. This in turn causes the depletion of analyte near the membrane surface which results in the so-called "super-Nernstian" response. The ISE becomes nonresponsive to further changes in analyte concentration below the super-Nernstian level.

To overcome these problems, several researchers have focused on controlling the transmembrane ionic flux to improve the LDLs.[18,21−24] Traditional approaches for transmembrane ionic flux control is actualized through the application of an external current opposing the direction of the ionic flux through the ion-selective membrane. In doing so, the concentration of analyte in the sample is not depleted and a stable reading at very low concentrations is achieved. Although using this method has resulted in the improvement of LDL by over 2 orders of magnitude, it is not a very practical technique for on-site detection as the magnitude of external current to be applied is often unknown. Moreover, application of the wrong currents can cause ion flux reversal, that is, ion flux from the internal filling

DOI: 10.1021/acs.analchem.8b00841
Anal. Chem. XXXX, XXX, XXX−XXX

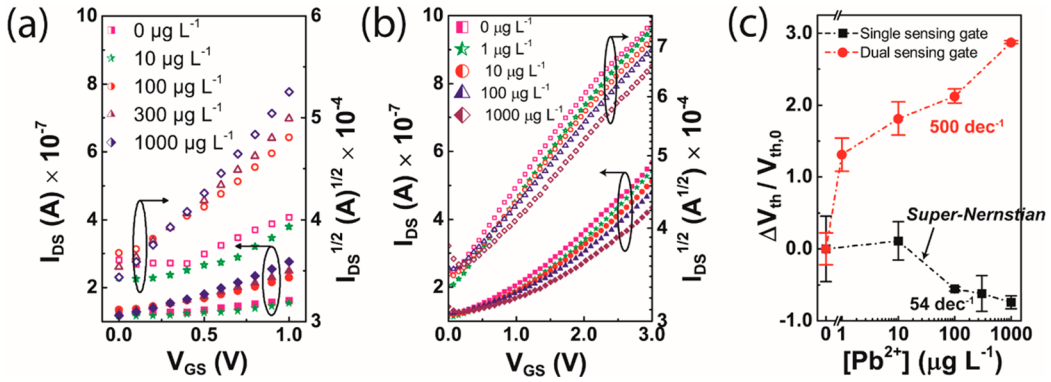

Figure 2. Experimental results. (a) TFT transfer curves for different concentrations of Pb^{2+} ranging from 0 to 1000 $\mu g\ L^{-1}$ in the single sensing gate. (b) TFT transfer curves for different concentrations of Pb^{2+} ranging from 0 to 1000 $\mu g\ L^{-1}$ in the dual sensing gate. (c) Calibration curve, as a function of normalized threshold voltage, of Pb^{2+} for both models.

solution to the sample, leading to sample contamination and membrane leaching.

A variant of ion selective electrodes is the ion selective field effect transistor (ISFET), where the metal gate electrode of a conventional field effect transistor is replaced with an ion selective membrane. ISFETs provide an in-built signal amplification feature, do not require the use of fragile glass bodies and are ideal for on-site sensing. However, ISFETs suffer from the same issues that plague the conventional ISE, such as high LDL, that hinder their use for monitoring of heavy metals. In this study, we apply the transmembrane ionic flux control approach to improve the LDL performance of ISFETs. To this end, we fabricated a dual sensing gated field effect transistor for the detection of Pb^{2+}. The results show a LDL improvement of two orders magnitude compared to the traditional one sensing gate ISFET. The improvement in LDL to 1 $\mu g\ L^{-1}$, which is below the WHO guideline limit, renders the sensor applicable for on-site Pb^{2+} monitoring. Furthermore, the system is analyzed using the Planck−Nernst−Poisson model to confirm the enhanced sensitivity.

DEVICE STRUCTURE AND MEASUREMENT TECHNIQUES

Figure 1a and 1b shows the two ISFET architectures compared in this study. In both cases, unit labeled TFT represents a thin film transistor fabricated on heavily doped Si substrate using thin film technology and n-type organic semiconductor. In Figure 1a, the unit labeled ISE is a Pb^{2+} SCISE assembled on a heavily doped Si substrate. The SCISE composed of a PVC matrix ISE, poly(3,4-ethylenedioxythiophene) (PEDOT): Cl conducting polymer solid contact layer. The heavily doped Si substrate of the TFT, which forms the bottom gate terminal, is connected to the heavily doped Si substrate of the ISE. A pseudo-reference electrode (Au probe wire) is immersed into the sample on the ISE. The gate voltage is supplied through the pseudoreference electrode and the source-drain current is recorded from the terminals of the TFT. The change in analyte concentration is transduced into a threshold voltage shift. In Figure 1b, SP1 and SP2 represent "sensing pad 1" and "sensing pad 2" and are identical to ISE from Figure 1a. However, in this setup, SP1 and SP2 are placed on a copper plate which puts them electrically in series. Samples with identical analyte concentrations are dropped on both SP1 and SP2. The gate voltage is supplied through the pseudoreference electrode on SP1 while the pseudoreference electrode on SP2 is connected to the bottom gate terminal of the TFT. The source-drain currents are recorded from the TFT terminals and the analyte concentration changes are reflected through a threshold voltage shifts. For further details on fabrication procedures, refer to the Supporting Information.

RESULTS AND DISCUSSION

Experimental Results. The *n*-channel TFT operates in accumulation mode. The TFT has a high-κ metal oxide dielectric layer, which keeps a low threshold voltage of 0.3 V (see Figure S4). This is done to prevent the immersed pseudoreference electrode, which supplies the gate voltage, from electrolyzing the sample.

Before the acquisition of the calibration curve, the ISE, SP1 and SP2 were preconditioned in a 2-step process: (i) at least 12 h in a 1 g L^{-1} (1000 ppm) $Pb(NO_3)_2$ (2% HNO_3) solution and (ii) at least 24 h in a 10 $\mu g\ L^{-1}$ (10 ppb) $Pb(NO_3)_2$ (2% HNO_3) solution.

The first step was undertaken to saturate the membrane with Pb(II) ion while the second step was undertaken to remove the excess $Pb(NO_3)_2$ coextracted into the membrane and reduce the transmembrane fluxes out of the membrane.[15,17]

The results from the calibration test are presented in Figure 2. The voltage was swept from 0 to 1 V in the single sensing gate ISFET and from 0 to 3 V in the dual sensing gate ISFET. This was done as the I_{DS} of single sensing gate ISFET becomes unstable beyond 1.5 V. However, in the case of the dual sensing gate model as 1 V is less than the threshold voltage, the voltage was scanned from 0 to 3 V. As shown in Figure 2a, in the single sensing gate model, the increase in concentration produces a decrease in threshold gate voltage. This is in agreement with previous studies where the threshold voltage of the *n*-channel organic field effect transistors (OFET) decreases as the concentration of the cation analyte increases.[25] Additionally, distinguishable transfer curves from the 0 $\mu g\ L^{-1}$ are observed only after the Pb^{2+} concentration is increased to 100 $\mu g\ L^{-1}$, making 100 $\mu g\ L^{-1}$ the LDL for this model. For the dual sensing gate model, the relationship between the normalized threshold voltage and the analyte concentration is inversed (Figure 2b). This is due to polarity reversal of the electrode supplying the voltage to the bottom gate of the TFT. In addition, the dual sensing gate model yields distinguishable transfer curves between 0 and 1 $\mu g\ L^{-1}$, which makes 1 $\mu g\ L^{-1}$ Pb^{2+} the LDL of this setup.

The calibration curve, as a function of the normalized threshold voltage, is presented in Figure 2c. For the single sensing gate model, there is no difference in threshold voltage

DOI: 10.1021/acs.analchem.8b00841
Anal. Chem. XXXX, XXX, XXX−XXX

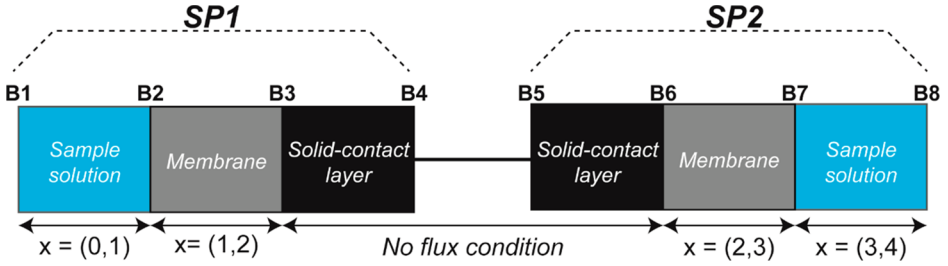

Figure 3. Schematic depiction of the 1-D model numerically solved using PNP equation. B1−B8 describes the boundaries between the layers of the SCISEs.

between 0 and 10 μg L^{-1}. This is possibly due to the "super-Nernstian" behavior which is observed as a steep slope between 10 and 100 μg L^{-1} in the calibration curve. The threshold voltage starts decreasing with increasing concentration beyond 100 μg L^{-1}. The linear slope of the calibration curve between 100 and 1000 μg L^{-1} (the working range) is 54 decade^{-1}. Meanwhile, the linear slope in the dual sensing gate model is 500 decade^{-1}. The calibration curve is linear between the 1 and 1000 μg L^{-1}. So, the dual sensing gate ISFET has a LDL 2 orders of magnitude lower than the single sensing gate ISFET. In addition, the sensitivity of the dual sensing gate ISFET is 10 times better than that of the single sensing gate ISFET.

Modeling Using the PNP Model. For simplicity, we restrict our consideration on a one-dimensional space with three intervals in each of the two ion-selective electrodes. We then study the 1-D Nernst−Planck equation which characterizes the change rate of ion concentration $c_i(x, t)$ with respect to the spatial gradient of the ion flux

$$J_i(x, t) = -D_i\left[\frac{\partial c_i(x, t)}{\partial x} + \frac{F}{RT} z_i c_i(x, t) E(x, t)\right] \quad (1)$$

Here, D_i and z_i denote the diffusion coefficient and valence of i-th ion, respectively. F, R, and T correspond to the Faraday's constant, the universal gas constant, and the absolute temperature, respectively. $E(x, t)$ is the electric field, which is to be solved from the Poisson equation

$$\varepsilon_r \frac{\partial E(x, t)}{\partial x} = \mathrm{P}(x, t) \quad (2)$$

where ε_r is the relative permittivity and $\mathrm{P}(x, t) = \Sigma z_i c_i(x, t)$ is the charge density. The electric potential (φ) can be simply obtained by an integration of the following equation:

$$-\frac{\mathrm{d}\varphi(x, t)}{\mathrm{d}x} = E(x, t) \quad (3)$$

In the sample solution, there are two movable ions: p^{2+} and n^- (representing Pb^{2+} and NO_3^-); while in the membrane, the concentration of negative ion is constant everywhere and can be treated as a fixed charge. In the conducting polymer, the electric field and electric potential are assumed to be constants. The boundary conditions and jump conditions are given as follows (see Figure 3): (1) In the far end of sample solution B1/B8, we assume fixed electroneutral ion concentrations and zero electric field. (2) Between sample and membrane B2/B7, we assume that the flux of negative ion is zero, the flux of positive ion is continuous, and the electric field is proportional to the reciprocal of permittivity. (3) Between membrane and conducting polymer B3/B6, we assume no flux in positive ion. In numerical simulation, we fix the electric potential and choose different ion concentrations on the boundary B1, and solve the electric potentials on B3 (single sensing gate potential) and B8 (dual sensing gate potential) respectively. The numerical simulation was carried out using MATLAB.

The parameters for the numerical simulation are given in Table 1.

Table 1. Parameters Used in Numerical Simulation

parameter	value
p^{2+} charge number (z_p)	+2
n^- charge number (z_n)	−1
sample solution ε_r	0.1
membrane ε_r	0.05
electric potential φ (B1)	3
electric field E (B1)	0
p^{2+} concentration	see footnote[a]
n^- concentration	see footnote[a]
electric potential φ initial value	0

[a]The numerical simulation study was performed for four logarithmically increasing bulk concentrations of p^{2+} and n^-

Results from Numerical Simulation. The distribution of p^{2+} and n^- ions within the system are shown in Figure 4a. As expected, the electroneutrality condition is observed everywhere except in Debye layer at the solution/membrane and the membrane/conductor interfaces. The time dependent electric potential developed at the gate terminal in the one sensing gate model (Ψ_1) and the dual sensing gate model (Ψ_2) are presented in Figure 4b. The calibration curve for p^{2+} ion is extracted in terms of Ψ at steady state is presented in Figure 4c. The average slope developed by the single sensing gate is 0.35 arb. units decade^{-1}, while the average slope value of the dual sensing gate is −0.65 arb. units decade^{-1}. This enhanced sensitivity especially at lower concentrations can be more easily distinguished via a field effect transistor.

Intuitatively, it is expected that the dual sensing gate arrangement, upon symmetrically placing in series; the net potential change should be zero. However, there is an asymmetricity in the electric field in the two sensor pads. This is because the gate voltage is applied to only one sensing pad whereas the other sensing pad is connected to a floating electrode. This difference in electric field results in the response from the dual sensing gate sensor.

The enhanced sensitivity of the dual sensing gate model can be explained by similar studies in which an ion-selective membrane is biased by small currents to control the depletion of analyte ions near the surface of the membrane.[18,21−24] The direction of the applied current opposes the ion flux. Because of this, the analyte ions in the sample solution near the membrane surface are not depleted as much thereby avoiding the super-Nernstian

DOI: 10.1021/acs.analchem.8b00841
Anal. Chem. XXXX, XXX, XXX−XXX

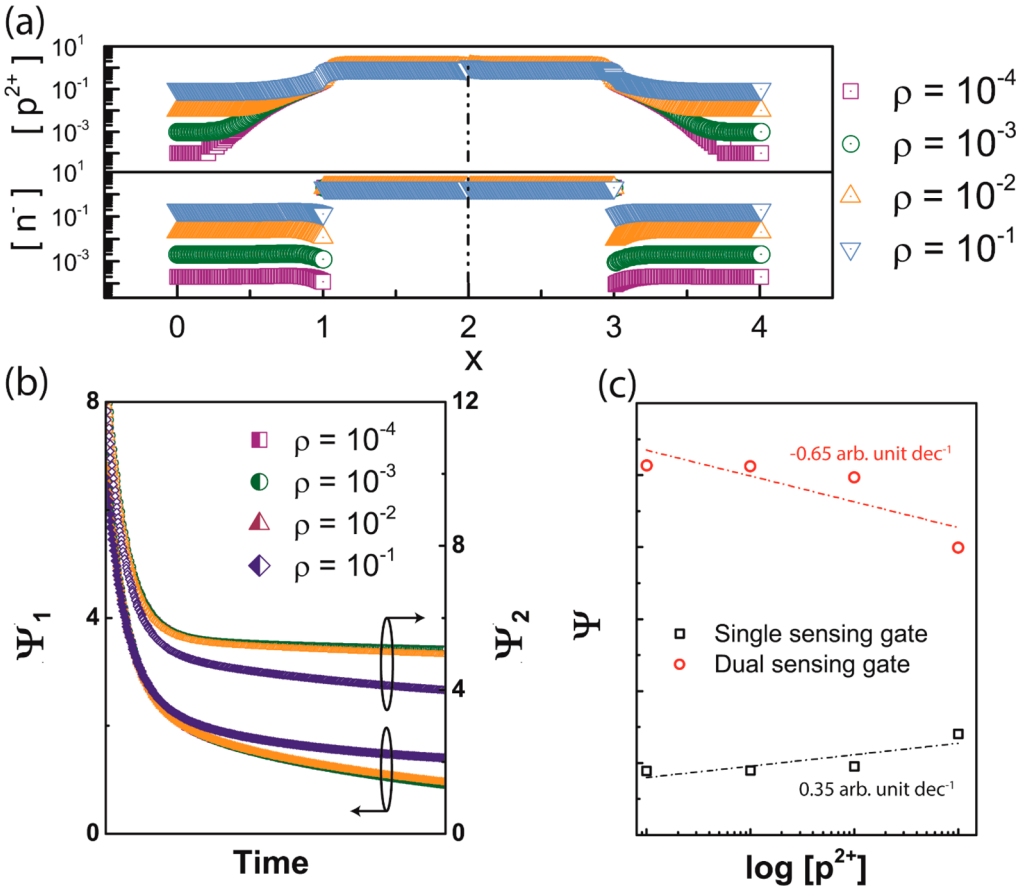

Figure 4. Numerical simulation data. (a) The concentration profiles for the p^{2+} and n^{-} across the system for four logarithmically increasing bulk concentrations. The dashed line in the middle represents the layers between B3−B6 connecting the two sensing gates. (b) Time-dependent electric potentials for the single sensing gate (Ψ_1) and the dual sensing gate (Ψ_2) systems for 4 logarithmically increasing concentrations. (c) Steady-state (t = 2000 time steps) electric potentials (Ψ) vs corresponding p^{2+} concentrations, that is, calibration curves for single and dual sensing gate models.

response. In the study by Michalska et al.,[24] a small current in the nano ampere range is applied against the flux of ions from the sample toward the solid contact resulting in the reduction of the slope of the analyte concentration gradient within the membrane. Thus, the depletion of ions from near the membrane surface is prevented and a lower limit is achieved. The practical limitation of this method is that the current required to achieve the lower detection limit is unknown a priori. With our method described here, this problem is overcome. The coupling of two sensing gates allows for the suppression of ion-flux through a "self-balanced" method.

To prove this proposed mechanism, the surface potential of the membrane is measured using Kelvin probe force microscopy (KPFM). The results of the KPFM study are presented in Figure 5a−d. Since this technique is not sensitive to changes in surface potential in the μg L^{-1} range, we used Pb^{2+} solutions mg L^{-1} range instead. The surface potential of the ISM with 10 mg L^{-1} is +32.1 mV in the single sensing gate model, while it decreases to −159.0 mV in the dual sensing gate model. Similarly, for 1000 mg L^{-1}, the average surface potential decreases from +72.7 mV in the single sensing gate model to +47.5 mV in the dual sensing gate model. The reduction of electric potential at the surface of the membrane is caused by the reduction of ion flux.[24] The mechanism schematic of the explanation is illustrated in Figure 5e−f. In this figure, the complexation and decomplexation of the mobile cation and the ionophore are represented by the forward and reverse reactions, respectively. Application of a voltage (which is represented by a green arrow in Figure 5f) in the opposite direction to that of the ion flux caused by the forward reaction, results in the suppression of the analyte ion depletion from the surface of the ion-selective membrane. This voltage is a result of the forward reaction at the second ion-selective membrane in the dual sensing gate model.

CONCLUSION

Experimentally, we demonstrate a detection limit of 1 μg L^{-1} using the dual gated structure and it is well within the WHO guideline limit of 10 μg L^{-1}. This unique sensor design is modeled by numerically solving the Planck-Nernst-Poisson equations. The solutions give insights into mechanisms behind the low detection limit of this sensor. We believe the reason behind the improvement in LDL lies primarily in suppression of the membrane fluxes due to the coupling of membrane potentials. Additionally, PNP model results reveal that on the dual sensing gate ISFET, the sensitivity of sensor increases by a factor of ∼10. The experimental implementation agreed in principle with the results of the numerical simulations.

Being based on robust non-aptasensor FET technology, we believe that this sensor fulfills the requirements (i.e., low detection limit, high sensitivity, nonfragile, etc.) to be used as an on-site prescreener complementary to the conventional laboratory-based analytical techniques.

DOI: 10.1021/acs.analchem.8b00841
Anal. Chem. XXXX, XXX, XXX−XXX

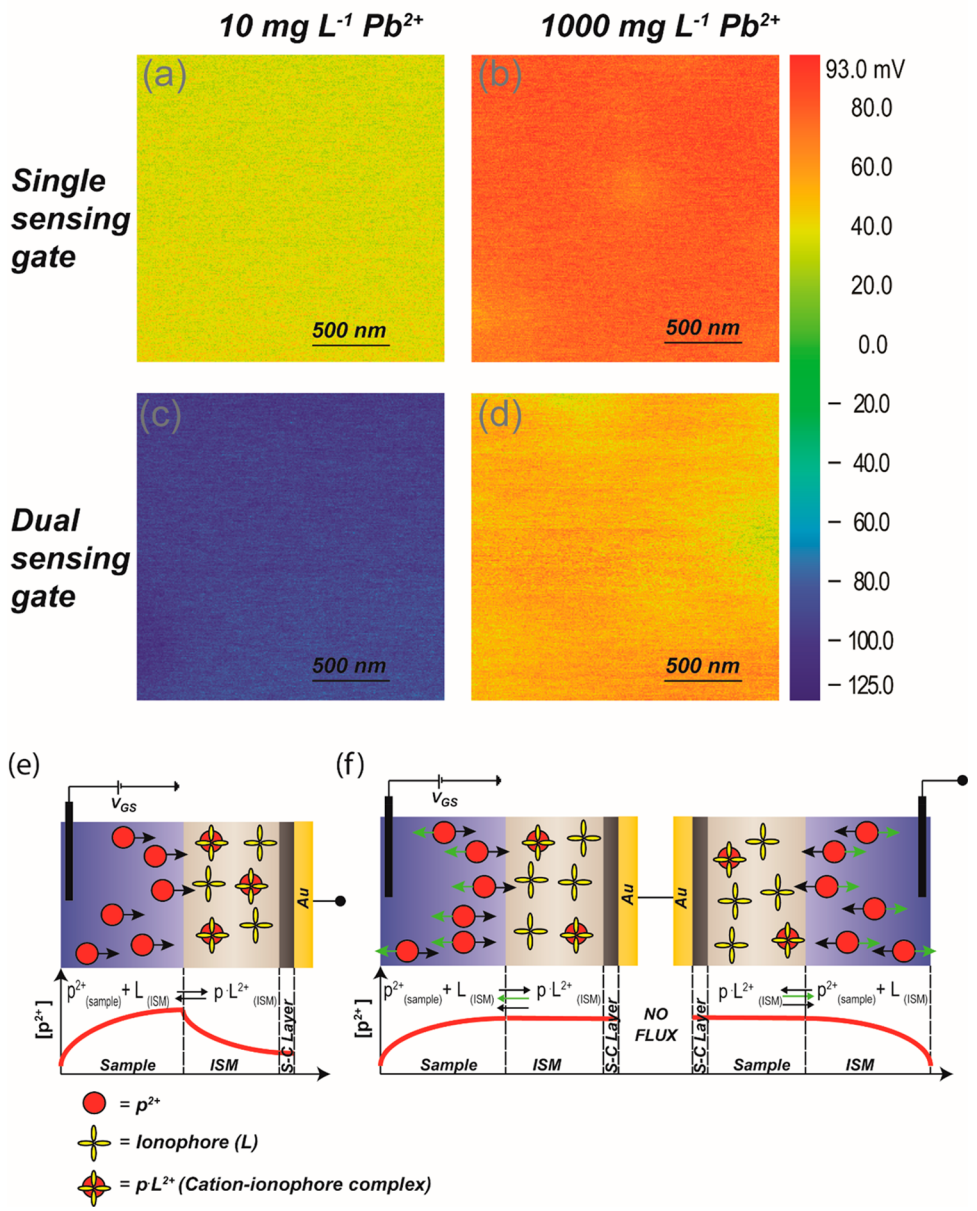

Figure 5. KPFM of ISM in single sensing gate model exposed to (a) 10 and (b) 1000 mg L^{-1} Pb^{2+} solutions. KPFM of ISM in dual sensing gate model exposed to (c) 10 and (d) 1000 mg L^{-1} Pb^{2+} solutions. Schematic of mechanism. The illustration of concentration profile of the p^{2+} ion in (e) single sensing gate model (f) dual sensing gate model as a function of position. ISM is the ion selective membrane. The effect of potential of the second gate on the first gate is represented by a green arrow on the p^{2+} ions in panels f.

■ ASSOCIATED CONTENT

Supporting Information

The Supporting Information is available free of charge on the ACS Publications website at DOI: 10.1021/acs.analchem.8b00841.

Materials, methods for fabrication, methods for testing, OFET transfer characteristics, and selectivity vs Cu^{2+} (PDF)

■ AUTHOR INFORMATION

Corresponding Author

*E-mail: val.roy@cityu.edu.hk.

ORCID

Vellaisamy A. L. Roy: 0000-0003-1432-9950

Notes

The authors declare no competing financial interest.

■ ACKNOWLEDGMENTS

We would like to acknowledge Mr. Daniel Yau for technical support. This work was supported by the Research Grant Council of HKSAR Project number T42-103/16N.

■ REFERENCES

(1) Tchounwou, P. B.; Yedjou, C. G.; Patlolla, A. K.; Sutton, D. J. In *Molecular, Clinical and Environmental Toxicology: Vol. 3: Environmental Toxicology*; Luch, A., Ed.; Springer Basel: Basel, 2012; p 133.

(2) Järup, L. *British medical bulletin* **2003**, *68*, 167.

(3) Payne, M. *Canadian Medical Association Journal* **2008**, *179*, 253.

(4) World Health Organization. *Guidelines for Drinking-Water Quality*, Vol. *1*; World Health Organization, 2004.

DOI: 10.1021/acs.analchem.8b00841
Anal. Chem. XXXX, XXX, XXX−XXX

(5) Maria das Graças Korn, A.; de Andrade, J. B.; de Jesus, D. S.; Lemos, V. A.; Bandeira, M. L.; dos Santos, W. N.; Bezerra, M. A.; Amorim, F. A.; Souza, A. S.; Ferreira, S. L. *Talanta* **2006**, *69*, 16.
(6) Lu, H.; Mou, S.; Yan, Y.; Tong, S.; Riviello, J. *J. Chromatogr. A* **1998**, *800*, 247.
(7) Soylak, M.; Aydin, F. A.; Saracoglu, S.; Elci, L.; Dogan, M. *Polym. J. Environ. Stud.* **2002**, *11*, 151.
(8) de Almeida Pereira, L.; de Amorim, I. G.; da Silva, J. B. B. *Talanta* **2004**, *64*, 395.
(9) Schock, M. R.; Hyland, R. N.; Welch, M. M. *Environ. Sci. Technol.* **2008**, *42*, 4285.
(10) Duarte, K.; Justino, C. I.; Freitas, A. C.; Gomes, A. M.; Duarte, A. C.; Rocha-Santos, T. A. *TrAC, Trends Anal. Chem.* **2015**, *64*, 183.
(11) Barton, J.; García, M. B. G.; Santos, D. H.; Fanjul-Bolado, P.; Ribotti, A.; McCaul, M.; Diamond, D.; Magni, P. *Microchim. Acta* **2016**, *183*, 503.
(12) Niu, X.; Lan, M.; Zhao, H.; Chen, C.; Li, Y.; Zhu, X. *Anal. Lett.* **2013**, *46*, 2479.
(13) Ribeiro, L. F.; Masini, J. C. *Electroanalysis* **2014**, *26*, 2754.
(14) Sokalski, T.; Ceresa, A.; Zwickl, T.; Pretsch, E. *J. Am. Chem. Soc.* **1997**, *119*, 11347.
(15) Anastasova, S.; Radu, A.; Matzeu, G.; Zuliani, C.; Mattinen, U.; Bobacka, J.; Diamond, D. *Electrochim. Acta* **2012**, *73*, 93.
(16) Sutter, J.; Radu, A.; Peper, S.; Bakker, E.; Pretsch, E. *Anal. Chim. Acta* **2004**, *523*, 53.
(17) Mathison, S.; Bakker, E. *Anal. Chem.* **1998**, *70*, 303.
(18) Bakker, E.; Pretsch, E. *TrAC, Trends Anal. Chem.* **2005**, *24*, 199.
(19) Bakker, E.; Telting-Diaz, M. *Anal. Chem.* **2002**, *74*, 2781.
(20) Bakker, E.; Pretsch, E. *Anal. Chem.* **2002**, *74*, 420A.
(21) Taillades, G.; Valls, O.; Bratov, A.; Dominguez, C.; Pradel, A.; Ribes, M. *Sens. Actuators, B* **1999**, *59*, 123.
(22) Sokalski, T.; Ceresa, A.; Fibbioli, M.; Zwickl, T.; Bakker, E.; Pretsch, E. *Anal. Chem.* **1999**, *71*, 1210.
(23) Szigeti, Z.; Vigassy, T.; Bakker, E.; Pretsch, E. *Electroanalysis* **2006**, *18*, 1254.
(24) Michalska, A.; Dumańska, J.; Maksymiuk, K. *Anal. Chem.* **2003**, *75*, 4964.
(25) Ji, S.; Sun, Q.-J.; Venkatesh, S.; Yan, Y.; Zhou, Y.; Zhuang, J.; Zhou, L.; Han, S.; Xu, Z.-X.; Roy, V. A. L. In *Oxide-Based Materials and Devices VII*; SPIE, 2016.

DOI: 10.1021/acs.analchem.8b00841
Anal. Chem. XXXX, XXX, XXX−XXX